Tenth International Conference on Computational Fluid Dynamics (ICCFD10), Barcelona,Spain, July 9-13, 2018

ICCFD10-323

Assessment of low Mach discretisation strategies for a turbulent channel flow with large density ratios

A. Both*, O. Lehmkuhl* and D. Mira*
Corresponding author: ambrus.both@bsc.es

* Barcelona Supercomputing Center (BSC), Barcelona, Spain.

The low Mach formulation of the coupled Navier-Stokes and energy equations proved to be a suitable tool for including variable density effects in thermal flow calculations, yet avoiding the high computational expenses that arise with a fully compressible formulation. In this paper we present the validation of such a low Mach solver developed in the parallel multi-physics simulation code: Alya. The LES solver is applied for fully developed anisothermal channel flow characterised by moderate Reynolds-numbers, and high density gradients.

Keywords: low Mach; channel flow; LES

1 Introduction

Simulation of flows characterised by low Mach number, moderate Reynolds number, and high density gradients are of high importance in combustion, which is one of the main interest of the authors. In combustion applications temperature differences of $O(10^3$ K) occur over distances of $O(10^{-4}$ m), while the transport properties strongly depend on temperature, and the velocities are moderate to facilitate a stable flame. The fully developed anisothermal channel flow introduced by Nicoud [1] is simulated to validate the low Mach solver.

This type of flow was studied using direct numerical simulation (DNS) [1, 2, 3], and large eddy simulation (LES) [4, 5, 6, 7, 8, 9] by different groups. Nicoud [1] studied DNS of anisothermal channel flow at a wall Reynolds number of $Re_\tau = 180$ with temperature ratio of $Tr = 2$ (ratio of upper and lower wall temperatures.) Toutant and Bataille [3] also use DNS to simulate a $Tr = 2$ case but at $Re_\tau = 395$, they argue that results in [1] are affected by low Reynolds number effects near the hot wall. Wang And Pletcher [4] executed LES of a channel at $Tr = 3$ with $Re_\tau = 180$ to study the effect of heat flux on the near wall turbulent structures. Lessani And Papalexandris [5] used LES to explore $Tr = 2$ and $Tr = 8$ at $Re_\tau = 180$ for validation purposes. Gravemeier and Wall [6] used a finite element LES to simulate the $Tr = 2$, $Re_\tau = 180$ case also with the aim of validation. Serra et al. [7] used LES for the study of the turbulent kinetic energy spectrum of anisothermal channels of $Tr \in \{2, 5\}$ and $Re_\tau \in \{180, 395\}$. Avila et al. [8] simulate a channel of $Tr = 2$ and $Re_\tau = 180$ for validating LES with finite element method. Aulery et al. [9] used both DNS and LES to investigate the turbulent kinetic energy balance of anisothermal channel flows at $Tr = 2$ and $Re_\tau \in \{180, 395\}$.

In this work simulations of anisothermal channel flows of $Tr = 2$ and $Re_\tau = 395$ are presented for the validation of the developed low Mach solver. The modelling approach and the details of the case are presented in section 2 and section 3. The results are discussed in 4.

2 Modelling approach

$Ma \ll 1$ indicates instantaneous acoustic equilibrium, since the velocity scale of the flow is much lower than the speed of sound. In the simulation acoustics are neglected by decomposing the pressure (P) to a spatially

homogeneous thermodynamic pressure (P_0) and the hydrodynamic pressure (p):

$$P(x,y,z,t) = P_0(t) + p(x,y,z,t) \tag{1}$$

The acoustics are eliminated by decoupling the density and the hydrodynamic component of the pressure, i.e.: the equation of state is evaluated using only the thermodynamic pressure. In this study ideal gas law is used keeping in mind the future combustion applications:

$$\rho = P_0 \frac{W}{R_u T} \tag{2}$$

where ρ is the density, W is the mean molecular weight of the gas, R_u is the universal gas constant, and T is the absolute temperature.

In open boundary problems the thermodynamic pressure is fixed throughout the domain, however in closed systems like the bi-periodic channel flow of this study, mass conservation constrains the thermodynamic pressure. The total mass in the closed domain denoted by Ω is:

$$M = \int_\Omega \rho \mathrm{d}V = \int_\Omega P_0 \frac{W}{R_u T} \mathrm{d}V = P_0 \frac{W}{R_u} \int_\Omega \frac{1}{T} \mathrm{d}V \tag{3}$$

In a closed system the initial mass must be sustained, thus:

$$P_0(t) = \frac{M_{t=0} R_u}{W \int_\Omega \frac{1}{T} \mathrm{d}V} \tag{4}$$

2.1 Governing equations

Favre filtering is applied to avoid the closure of terms with subgrid density fluctuations:

$$\widetilde{\phi} = \frac{\overline{\rho\phi}}{\overline{\rho}} \tag{5}$$

where ϕ is an arbitrary quantity, and $\sim$ and – denote Favre and Reynolds filtering respectively. After filtering the low Mach approximation of the Navier-Stokes equations yields:

$$\frac{\partial \overline{\rho}}{\partial t} + \frac{\partial \overline{\rho} \widetilde{u_j}}{\partial x_j} = 0 \tag{6}$$

$$\frac{\partial \overline{\rho} \widetilde{u_i}}{\partial t} + \frac{\partial \overline{\rho} \widetilde{u_j} \widetilde{u_i}}{\partial x_j} = -\frac{\partial \overline{p}}{\partial x_i} + \frac{\partial \overline{\tau_{ij}}}{\partial x_j} - \frac{\partial \overline{\rho} \left(\widetilde{u_j u_i} - \widetilde{u_j} \widetilde{u_i} \right)}{\partial x_j} + f_i \tag{7}$$

$$\frac{\partial \overline{\rho} \widetilde{h}}{\partial t} + \frac{\partial \overline{\rho} \widetilde{u_j} \widetilde{h}}{\partial x_j} = \frac{\mathrm{d}P_0}{\mathrm{d}t} - \frac{\partial \overline{q_j}}{\partial x_j} - \frac{\partial \overline{\rho} \left(\widetilde{u_j h} - \widetilde{u_j} \widetilde{h} \right)}{\partial x_j} \tag{8}$$

where $\widetilde{u_j}$ is the resolved velocity, $\overline{\tau_{ij}}$ is the viscous stress tensor, f_i is an external force term, $\widetilde{h}$ is the resolved enthalpy, and $\overline{q_j}$ is the resolved heat flux vector. The viscous stress tensor is calculated as:

$$\overline{\tau_{ij}} = 2\overline{\mu} \widetilde{S}_{ij}^D \tag{9}$$

where $\widetilde{S}_{ij}^D = \widetilde{S}_{ij} - \frac{1}{3}\delta_{ij}\widetilde{S}_{kk}$ is the traceless part of the strain rate tensor with δ_{ij} being the Kronecker-delta, and the strain rate tensor is:

$$\widetilde{S}_{ij} = \frac{1}{2} \left(\widetilde{g}_{ij} + \widetilde{g}_{ji} \right) \tag{10}$$

with the velocity gradient tensor denoted by: $\widetilde{g}_{ij} = \frac{\partial \widetilde{u}_i}{\partial x_j}$.

The enthalpy is related to the temperature as:

$$\widetilde{h} = h_{ref} + \int_{T_{ref}}^{\widetilde{T}} c_p(\tau)\mathrm{d}\tau \tag{11}$$

where h_{ref} is a reference enthalpy, and T_{ref} is the corresponding reference temperature. The isobaric specific heat (c_p) can be temperature dependent. The heat flux vector is evaluated using Fourier's law of heat conduction:

$$\overline{q_j} = -\overline{\lambda}\frac{\partial \widetilde{T}}{\partial x_j} \tag{12}$$

Eq.(11) has to be inverted to evaluate the heat flux and the temperature dependent quantities ($\overline{\rho}, \overline{\mu}, \overline{\lambda}.$) In general this inversion is executed by a Newton–Raphson method, although in this work the specific heat is constant. Note that the viscous work $\left(\overline{\tau_{ij}}\frac{\partial \widetilde{u_i}}{\partial x_j}\right)$, the work of subgrid stresses $\left(\overline{\rho}\left(\widetilde{u_j u_i} - \widetilde{u_j}\widetilde{u_i}\right)\frac{\partial \widetilde{u_i}}{\partial x_j}\right)$, and the work of hydrodynamic pressure $\left(\widetilde{u_i}\frac{\partial \overline{p}}{\partial x_i}\right)$ is neglected in the enthalpy equation, as convection and conduction dominates the enthalpy transport in the intended applications.

2.2 Subgrid modelling

The subgrid terms in Eq.(7) and Eq.(8) are closed using eddy viscosity models:

$$\tau_{ij}^{sgs} = \overline{\rho}\left(\widetilde{u_j u_i} - \widetilde{u_j}\widetilde{u_i}\right) = -2\overline{\rho}\nu_t\widetilde{S_{ij}} \tag{13}$$

$$q_j^{sgs} = \overline{\rho}\left(\widetilde{u_j h} - \widetilde{u_j}\widetilde{h}\right) = -\overline{\rho}\frac{\nu_t}{Pr_t}\frac{\partial \widetilde{h}}{\partial x_j} \tag{14}$$

where: τ_{ij}^{sgs} is the subgrid stress tensor, q_j^{sgs} is the subgrid heat flux, ν_t is the eddy viscosity, and Pr_t is the turbulent Prandtl number. $Pr_t = 0.9$ is used in this study proposed in [10] and verified for the low Mach limit in [1, 3]. The eddy-viscosity model proposed by Vreman [11] is used in this work. The following symmetric tensor is defined incorporating the effect of anisotropic mesh size:

$$\beta_{ij} = \Delta_m^2 \widetilde{g}_{im}\widetilde{g}_{jm} \tag{15}$$

where Δ_m is the cell size in coordinate m. The second scalar invariant of β_{ij} tensor ($B_\beta = \beta_{11}\beta_{22} - \beta_{12}^2 + \beta_{11}\beta_{33} - \beta_{13}^2 + \beta_{22}\beta_{33} - \beta_{23}^2$) is used to define the eddy viscosity:

$$\nu_t^{Vreman} = c\left(\frac{B_\beta}{\widetilde{g}_{ij}\widetilde{g}_{ij}}\right)^{1/2} \tag{16}$$

where $c = 0.1$ is used in this study.

2.3 Spatial discretization

A finite element Galerkin approximation is used for the space discretisation with a non-incremental fractional step extended to low Mach to stabilize pressure. This allows for the use of finite element pairs that do not satisfy the inf-sup condition, such as equal order interpolation for the velocity and pressure used in this work. EMAC discretisation [12] is applied for the treatment of the convective term, which assures the simultaneous conservation of kinetic energy, momentum and angular momentum.

2.4 Temporal discretization

Temporal discretisation is performed through an explicit standard third-order Runge-Kutta scheme combined with an eigenvalue based time step estimator [13]. First the enthalpy is advanced through the Runge-Kutta

scheme. The enthalpy in the k^{th} sub-step is evaluated as:

$$\widetilde{h}^k = \widetilde{h}^n + \frac{\Delta t^n}{\overline{\rho}^{k-1}} \sum_{m=1}^{k} a_{km} \left(\left(-\frac{\partial \overline{\rho} \widetilde{u_j} \widetilde{h}}{\partial x_j} - \frac{\partial \overline{q_j} + q_j^{sgs}}{\partial x_j} \right)^m + \left(\frac{\mathrm{d}P_0}{\mathrm{d}t} \right)^n \right), \quad k = 1..s \tag{17}$$

The enthalpy in the next step is calculated as:

$$\widetilde{h}^{n+1} = \widetilde{h}^n + \frac{\Delta t^n}{\overline{\rho}^{k=s-1}} \sum_{k=1}^{s} b_k \left(\left(-\frac{\partial \overline{\rho} \widetilde{u_j} \widetilde{h}}{\partial x_j} - \frac{\partial \overline{q_j} + q_j^{sgs}}{\partial x_j} \right)^k + \left(\frac{\mathrm{d}P_0}{\mathrm{d}t} \right)^n \right) \tag{18}$$

where a_{km} and b_k are the coefficients of the Runge-Kutta scheme (See Tab.1.) The time derivative of the thermodynamic pressure is approximated at the end of each time step following the method in [14]:

$$\left(\frac{\mathrm{d}P_0}{\mathrm{d}t} \right)^{n+1} = \frac{1}{\Delta t^{n-1}} \left(\left(1 + \frac{\Delta t^n}{\Delta t^{n-1}} \right) P_0^n - \left(1 + \frac{\Delta t^n}{\Delta t^{n-1}} + \frac{\Delta t^n}{\Delta t^{n-2}} \right) P_0^{n-1} + \frac{\Delta t^n}{\Delta t^{n-2}} P_0^{n-2} \right) \tag{19}$$

For advancing the velocity field, the non-incremental fractional step method is combined with the Runge-Kutta scheme. The k^{th} sub-step could consist of:

$$\overline{\rho}^{k,*} \widetilde{u_i}^{k,*} = \overline{\rho}^n \widetilde{u_i}^n + \Delta t^n \sum_{m=1}^{k} a_{km} \left(-\frac{\partial \overline{\rho} \widetilde{u_j} \widetilde{u_i}}{\partial x_j} + \frac{\partial \widetilde{\tau_{ij}} + \tau_{ij}^{sgs}}{\partial x_j} + f_i \right)^m, \qquad k = 1..s \tag{20}$$

$$-\frac{\partial^2 \overline{p}^k}{\partial x_i^2} = \frac{1}{c_k \Delta t^n} \left(-\frac{\partial \overline{\rho}^k}{\partial t} - \frac{\partial \overline{\rho}^{k,*} \widetilde{u_i}^{k,*}}{\partial x_i} \right), \qquad k = 1..s \tag{21}$$

$$\overline{\rho}^k \widetilde{u_i}^k = \overline{\rho}^{k,*} \widetilde{u_i}^{k,*} - c_k \Delta t^n \frac{\partial \overline{p}^k}{\partial x_i}, \qquad k = 1..s \tag{22}$$

where c_k is also listed in Tab.1. The solution of the Poisson eqation (Eq.(21)) is very expensive. Solving it in the sub-steps is optional in the developed algorithm, this step can be omitted by directly using an approximate pressure field in Eq.(22). The velocity field in the next time step is calculated as:

$$\overline{\rho}^{n+1,*} \widetilde{u_i}^{n+1,*} = \overline{\rho}^n \widetilde{u_i}^n + \Delta t^n \sum_{k=1}^{s} b_k \left(-\frac{\partial \overline{\rho} \widetilde{u_j} \widetilde{u_i}}{\partial x_j} + \frac{\partial \widetilde{\tau_{ij}} + 2\overline{\rho} \nu_t \widetilde{S_{ij}}}{\partial x_j} + f_i \right)^k \tag{23}$$

$$-\frac{\partial^2 \overline{p}^{n+1}}{\partial x_i^2} = \frac{1}{\Delta t^n} \left(-\frac{\partial \overline{\rho}^{n+1}}{\partial t} - \frac{\partial \overline{\rho}^{n+1,*} \widetilde{u_i}^{n+1,*}}{\partial x_i} \right) \tag{24}$$

$$\overline{\rho}^{n+1} \widetilde{u_i}^{n+1} = \overline{\rho}^{n+1,*} \widetilde{u_i}^{n+1,*} - \Delta t^n \frac{\partial \overline{p}^{n+1}}{\partial x_i} \tag{25}$$

where: $\widetilde{u_i}^{n+1,*}$ is a pseudo velocity used in the fractional step method.

Instead of using the divergence of the momentum evaluated in the next time step $\left(\frac{\partial \overline{\rho}^{n+1} \widetilde{u_i}^{n+1}}{\partial x_i} \right)$ on the right hand side of the Poisson equation (Eq.(24)), this term is substituted by the time derivative of density (based on Eq.(6)), and it is calculated using the second order backward approximation proposed by Nicoud [15]:

$$\frac{\partial \overline{\rho}^{n+1}}{\partial t} = \frac{((\Delta t^n + \Delta t^{n-1})^2 - (\Delta t^k)^2) \overline{\rho}^{n+1} - (\Delta t^n + \Delta t^{n-1})^2 \overline{\rho}^n + (\Delta t^n)^2 \overline{\rho}^{n-1}}{\Delta t^n \Delta t^{n-1} (\Delta t^n + \Delta t^{n-1})} \tag{26}$$

c_k	a_{km}		
0			
1/2	1/2		
1	-1	2	
	1/6	2/3	1/6
		b_k	

Table 1: Constants of the standard third-order Runge-Kutta scheme

3 Application

Fig.1 illustrates the channel flow geometry. As commonly used, the stream-wise, wall-normal, and span-wise directions are aligned with the x, y, and z coordinates respectively. The channel half-height is chosen as $h = 1$ m. The cold and hot walls are located at $y_c = 0$ m and $y_h = 2$ m respectively. The stream-wise and span-wise sizes applied by Serra et al. [7] are adapted: $L_x = 2\pi h$, $L_z = \pi h$. The domain is periodic in the x and z directions.

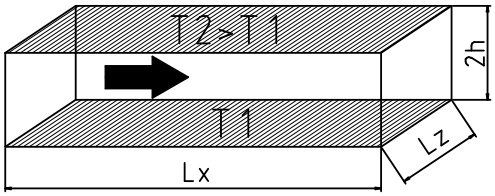

Figure 1: Channel geometry

The temperature dependent material properties of Toutant and Bataille [3] are used, as these represent realistic, gas-like behaviour. The gas constant is:

$$R = \frac{R_u}{W} = 287 \ \frac{\mathrm{J}}{\mathrm{kgK}} \tag{27}$$

The dynamic viscosity is calculated using Sutherland's law:

$$\mu = \frac{T^{3/2}}{T + 111 \ \mathrm{K}} 1.461 \cdot 10^{-6} \ \frac{\mathrm{Pas}}{\sqrt{\mathrm{K}}} \tag{28}$$

The specific heat is taken as constant: $c_p = 1005 \ \frac{\mathrm{J}}{\mathrm{kgK}}$, thus Eq.(11) is greatly simplified:

$$h = c_p T \tag{29}$$

The thermal conductivity is calculated assuming constant molecular Prandtl number ($Pr = 0.71$):

$$\lambda = \frac{\mu c_p}{Pr} \tag{30}$$

The mean flow is induced by applying a constant artificial pressure gradient (f_1) in the x direction. Following the convention of incompressible channel simulations the flow is characterised by the wall Reynolds number, however as the material properties are evaluated at the corresponding wall temperature:

$$Re_\tau = \frac{\rho_w u_\tau h}{\mu_w} \tag{31}$$

where "w" indicates the wall state ($\rho_w = \rho(P_0, T_w)$, $\mu_w = \mu(T_w)$), and u_τ is the friction velocity:

$$u_\tau = \sqrt{\frac{\langle \tau_w \rangle}{\rho_w}} \tag{32}$$

with $\langle \tau_w \rangle$ being the mean wall shear stress calculated as:

$$\langle \tau_w \rangle = \frac{1}{\Delta t} \sum_{t_0}^{t_0+\Delta t} \frac{|F_{w,x}(t_i)|}{A_w} \mathrm{d}t_i \tag{33}$$

where $F_{w,x}(t_i)$ is the friction force exerted on the wall at time step i, A_w is the wall surface, Δt is length of the averaging interval, and $\mathrm{d}t_i$ is the time step size.

The two walls have different wall Reynolds numbers for non-unity temperature ratios. The usual approach to reach different temperature ratios is keeping the cold wall as it is while increasing the temperature of the hot wall. If Sutherland's law is applied, the viscosity at the hot wall increases, and the wall Reynolds number decreases. The cases can be characterised by the average wall Reynolds number:

$$Re_\tau = \frac{Re_{\tau,c} + Re_{\tau,h}}{2} \tag{34}$$

"c" and "h" indicating the cold and hot walls.

There are numerous approaches in the literature for comparing different temperature ratios. The DNS database considered in this work imposes a force term such that the average wall Reynolds number is constant [3], thus the force term is expressed as:

$$f_1 = \frac{\tau_c + \tau_h}{2h} = \frac{\frac{Re_{\tau,c}^2 \mu_c^2}{\rho_c} + \frac{Re_{\tau,h}^2 \mu_h^2}{\rho_h}}{2h^3} \tag{35}$$

To calculate the force term in the $Tr = 2$ case the two wall Reynolds numbers are taken from the DNS [3] a priori: $Re_{\tau,c} = Re_{\tau,c}^{DNS} = 235$ and $Re_{\tau,h} = Re_{\tau,h}^{DNS} = 565$. The temperature scaling is based on the wall heat flux ($\dot{q}_w$), the friction temperature is defined as:

$$T_\tau = \frac{\dot{q}_w}{\rho_w c_p u_\tau} \tag{36}$$

Structured hexahedral mesh is applied with homogeneous size in x and z. The mesh is refined in the wall-normal direction using the formula in [3]. The node coordinates are calculated as:

$$y_i = h \left\{ 1 + \frac{1}{\alpha} \tanh \left[\mathrm{atanh}(\alpha) \left(\frac{2i}{N_{ey}} - 1 \right) \right] \right\}, \qquad i = 0..N_{ey} \tag{37}$$

where N_{ey} is the number of elements in y, and α is a parameter expressing the level of refinement. The number of hexahedral elements in the corresponding directions is set to $165 \times 123 \times 82$. A refinement parameter of $\alpha = 0.983$ is used, thus at the wall distance of the first node in wall units is $\Delta_{y,min}^+ = 0.54$, while $\Delta_x^+ \approx \Delta_{y,max}^+ \approx \Delta_z^+ \approx 15$ assuming $Re_\tau = 395$.

4 Results

4.1 Validation at the incompressible limit

The performance of the solver is assessed at quasi-incompressible conditions $Tr = 1.01$ and $Re_\tau = 395$. The results are compared to the incompressible DNS of Moser et al. [16] in Fig.2. The match is considerably good, the remaining discrepancies could be decreased by further mesh refinement.

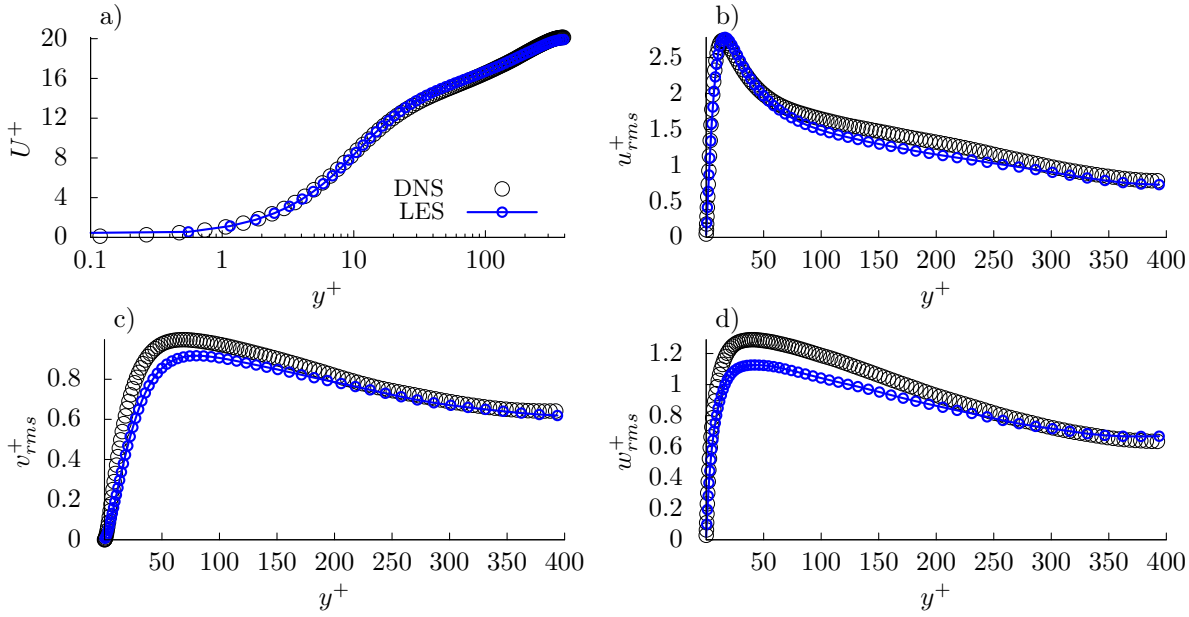

Figure 2: Comparison of mean velocity and fluctuations at the incompressible limit ($Re_\tau = 395, Tr = 1.01$), a: mean stream-wise velocity, b: stream-wise velocity RMS, c: wall-normal velocity RMS, d: span-wise velocity RMS, DNS: Moser et al. [16]

4.2 Validation at Tr = 2

The results of $Tr = 2$ and $Re_\tau = 395$ are compared to the DNS of Toutant and Bataille [3] in Fig.3. The wall Reynolds numbers predicted by the present work are $Re_{\tau,c} = 516$ and $Re_{\tau,h} = 287$ on the cold and hot walls respectively. The discrepancies of the mean velocity and temperature present in Fig.3, could originate from the different wall units (different scaling.) Also the cold side becomes more turbulent, thus the same mesh has a lower quality at the increased temperature ratio. It is worth pointing out, that the wall-normal and span-wise fluctuations have the most noticeable differences even in the quasi-incompressible case (Fig.2) and these discrepancies are expected to increase with the temperature ratio. Overall the general trends are well predicted.

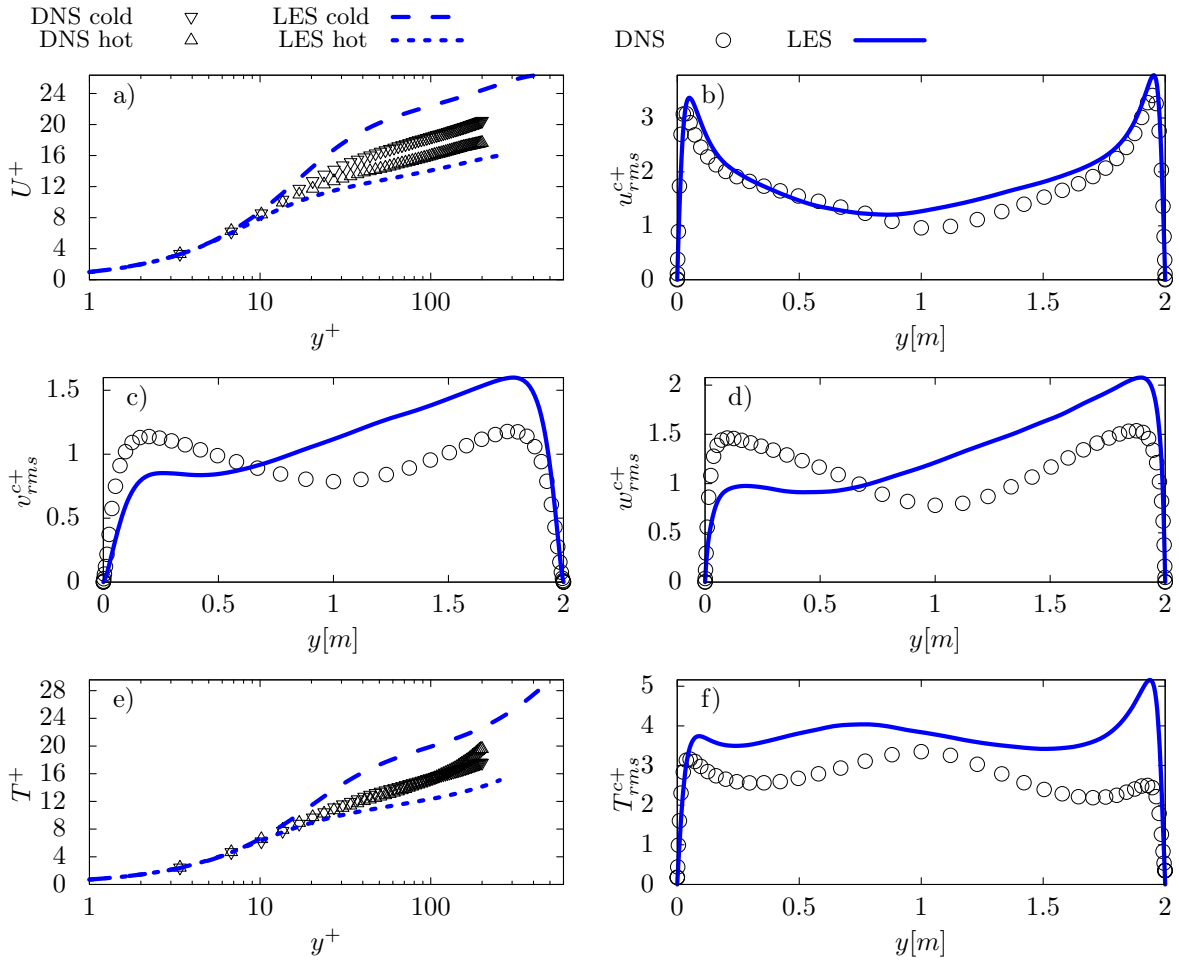

Figure 3: Comparison of mean and RMS properties of the case: $Re_\tau = 395, Tr = 2$, "$c+$" superscript indicates scaling by the cold wall units, a: mean stream-wise velocity, b: stream-wise velocity RMS, c: wall-normal velocity RMS, d: span-wise velocity RMS, e: mean temperature $\left(T^+ = \frac{T_w - \langle T \rangle}{T_\tau}\right)$, f: temperature RMS, DNS: Toutant and Bataille [3] (truncated at $y+ = 200$)

Acknowledgement

This project has received funding from the European Union's Horizon 2020 research and innovation programme under the Marie Skłodowska-Curie grant agreement No. 713673. Ambrus Both has received financial support through the "la Caixa" INPhINIT Fellowship Grant for Doctoral studies at Spanish Research Centres of Excellence, "la Caixa" Banking Foundation, Barcelona, Spain.

References

[1] FC Nicoud. Numerical study of a channel flow with variable properties. ctr annual research briefs 1998, 1999.

[2] Franck Nicoud and Thierry Poinsot. Dns of a channel flow with variable properties. In *TSFP DIGITAL LIBRARY ONLINE*. Begel House Inc., 1999.

[3] Adrien Toutant and Francoise Bataille. Turbulence statistics in a fully developed channel flow submitted to a high temperature gradient. *International Journal of Thermal Sciences*, 74:104–118, 2013.

[4] Wen-Ping Wang and Richard H Pletcher. On the large eddy simulation of a turbulent channel flow with significant heat transfer. *Physics of Fluids*, 8(12):3354–3366, 1996.

[5] Bamdad Lessani and Miltiadis V Papalexandris. Time-accurate calculation of variable density flows with strong temperature gradients and combustion. *Journal of Computational Physics*, 212(1):218–246, 2006.

[6] Volker Gravemeier and Wolfgang A Wall. An algebraic variational multiscale–multigrid method for large-eddy simulation of turbulent variable-density flow at low mach number. *Journal of Computational Physics*, 229(17):6047–6070, 2010.

[7] Sylvain Serra, Adrien Toutant, Francoise Bataille, and Ye Zhou. Turbulent kinetic energy spectrum in very anisothermal flows. *Physics Letters A*, 376(45):3177–3184, 2012.

[8] Matias Avila, Ramon Codina, and Javier Principe. Large eddy simulation of low mach number flows using dynamic and orthogonal subgrid scales. *Computers & Fluids*, 99:44–66, 2014.

[9] Frederic Aulery, Dorian Dupuy, Adrien Toutant, Françoise Bataille, and Ye Zhou. Spectral analysis of turbulence in anisothermal channel flows. *Computers & Fluids*, 151:115–131, 2017.

[10] PG Huang, GN Coleman, and P Bradshaw. Compressible turbulent channel flows: Dns results and modelling. *Journal of Fluid Mechanics*, 305:185–218, 1995.

[11] A W Vreman. An eddy-viscosity subgrid-scale model for turbulent shear flow: Algebraic theory and applications. *Physics of fluids*, 16(10):3670–3681, 2004.

[12] S. Charnyi, T. Heister, M. A. Olshankii, and L. G. Rebholz. On conservation laws of Navier-Stokes Galerkin discretizations. *J. Comput. Phys.*, 337:289–308, 2017.

[13] F. X. Trias and O. Lehmkuhl. A Self-Adaptive Strategy for the Time Integration of Navier-Stokes Equations. *Numerical Heat Transfer, Part B: Fundamentals*, 60(July 2013):116–134, 2011.

[14] Emmanuel Motheau and John Abraham. A high-order numerical algorithm for dns of low-mach-number reactive flows with detailed chemistry and quasi-spectral accuracy. *Journal of Computational Physics*, 313:430–454, 2016.

[15] Franck Nicoud. Conservative high-order finite-difference schemes for low-mach number flows. *Journal of Computational Physics*, 158(1):71–97, 2000.

[16] Robert D Moser, John Kim, and Nagi N Mansour. Direct numerical simulation of turbulent channel flow up to re τ= 590. *Physics of fluids*, 11(4):943–945, 1999.

[17] Juan C del Álamo and Javier Jiménez. Spectra of the very large anisotropic scales in turbulent channels. *Physics of Fluids*, 15(6):L41–L44, 2003.